Fermi National Accelerator Laboratory

FERMILAB-Conf-94/144-E

CDF

# Measurement of the SS-OS Dijet Cross-Section Ratio

The CDF Collaboration

*Fermi National Accelerator Laboratory*
*P.O. Box 500, Batavia, Illinois 60510*

June 1994

Submitted to the *27th International Conference on High Energy Physics*, Glasgow, Scotland, July 20-27, 1994

## Disclaimer

ICHEP94 Ref. gls0402
Submitted to Pa-11, Pl-13

CDF/PUB/JET/PUBLIC/2606
May 26, 1994
FERMILAB-CONF-94/144-E

# Measurement of the SS-OS Dijet Cross-Section Ratio

The CDF Collaboration *

**Abstract**

We present a measurement of the same-side to opposite side dijet cross section ratio in $p\bar{p}$ collisions at $\sqrt{s} = 1.8$ TeV, using approximately 19 pb$^{-1}$ of data collected by the Collider Detector at Fermilab during the 1992-93 run of the Fermilab Tevatron. We show that, for large pseudorapidities and small transverse energies, this ratio is sensitive to the gluon distribution at small x. We compare the measured values of the ratio with the theoretical predictions, smeared to incorporate detector effects, for a variety of parton distributions. Overall, we find very good agreement between the data and the predictions for a wide range of jet energies and pseudorapidities. At low transverse energies, there are some minor discrepancies between the data and the predictions that could arise from the effects of a more singular gluon distribution.

*Contact Eve Kovács, KOVACS@FNALD.FNAL.GOV
Submitted 27th International Conference on High Energy Physics, University of Glasgow, Glasgow, Scotland, July 20-27, 1994

# 1 Introduction

One of the largest uncertainties in the next-to-leading order QCD predictions for many processes arises from uncertainties in the behavior of the parton distributions. In particular, the gluon distribution at small momentum fraction $x$ is very poorly determined. Jet processes at the Fermilab Collider are sensitive to the gluon distribution at leading order, and hence can provide a direct measurement of this quantity for a wide range of $x$ and $Q^2$. Furthermore, the contribution to the jet cross section from the gluon distribution in a specific range of $x$ may be enhanced by restricting the kinematic regions in which the jets may lie. Then, by forming suitably defined ratios of such cross sections, it is possible to cancel some of the experimental and theoretical uncertainties in order to obtain precise measurements that are particularly sensitive to the gluon distribution in the desired range of $x$.

In this paper, we present preliminary results for a measurement of $R$, the ratio of the "same-side" (SS) and "opposite-side" (OS) two-jet differential cross sections for jet production in $p\bar{p}$ collisions at $\sqrt{s} = 1800$ GeV. The same-side (opposite-side) jet cross section is obtained by selecting events having jet configurations for which $\eta_1$ and $\eta_2$, the pseudorapidities of the two jets with the highest transverse energies, have the same absolute values and the same (opposite) signs. That is, the two leading jets are required to be on the same (opposite) side of the detector at the same value of $|\eta|$. This ratio has a number of advantages, both experimental and theoretical. Experimentally, some systematic errors, such as the normalization error on the luminosity and errors due to trigger efficiency corrections cancel. Theoretically, errors due to uncertainties in the choice of renormalization scales partially cancel. The ratio is interesting because for cases where both jets have low values of transverse energy, $E_T$, and high values of $|\eta|$, it provides a direct and sensitive probe of the value of the gluon distribution at small $x$.

A simple argument based on LO QCD shows how the small-$x$ sensitivity of $R$ comes about. For $2 \to 2$ scattering, given the transverse momentum $p_T$ and the rapidities $y_1$ and $y_2$ of the two final state partons, one can readily deduce the momentum fractions $x_a$ and $x_b$ of the incoming partons:

$$x_{a,b} = \sqrt{\tau}\exp(\pm y_{boost}), \tag{1.1}$$

where

$$\sqrt{\tau} = (2p_T/\sqrt{s})\cosh y^*, \tag{1.2a}$$

$$y^* = \tfrac{1}{2}(y_1 - y_2), \tag{1.2b}$$

$$y_{boost} = \tfrac{1}{2}(y_1 + y_2). \tag{1.2c}$$

Identifying the final state partons with the outgoing jets, we find that at CDF, by choosing jet configurations with $y_1 = y_2 = 2.5$, and $p_T = 20$ GeV, values as small as $x = .002$ can be easily reached.

Schematically, the two-jet differential cross section may be written as

$$\frac{d\sigma}{dy_1 dy_2 dp_T} \sim \sum_{ij} f_i(x_a, Q^2) f_j(x_b, Q^2) \hat{\sigma}_{ij}(p_T, y^*), \tag{1.3}$$

where the $f_i(x, Q^2)$ denote the parton distribution functions for partons of type $i$ ($i = u$, $\bar{u}$, ...) evaluated at momentum fraction $x$ and momentum scale $Q$, and the $\hat{\sigma}_{ij}$ denote the parton-parton cross sections for the scattering of partons $i$ and $j$. SS jet configurations have $y_{boost} = \bar{y}$ and $y^* = 0$. For large values of $|\bar{y}|$ and small values of $p_T$, the two-jet cross section in (1.3) is sensitive to the product of parton distributions, one evaluated at large $x$, $x_a = (2p_T/\sqrt{s})\exp(|\bar{y}|)$, and the other evaluated at small $x$, $x_b = (2p_T/\sqrt{s})\exp(-|\bar{y}|)$. Hence, for sufficiently extreme values of $|\bar{y}|$ and $p_T$, we expect the sum in (1.3) to be dominated by the contributions from gluon–valence-quark scattering, where the quark has $x = x_a$ and the gluon has $x = x_b$. Since the valence-quark distributions are well known at large $x$, the SS cross section is a direct measure of the gluon distribution at small $x$. On the other hand, OS jet configurations have $y_{boost} = 0$ and $y^* = \bar{y}$. In this case, the two-jet cross section is sensitive to the product of parton distributions both evaluated at $\bar{x} = (2p_T/\sqrt{s})\cosh\bar{y} = 1/2(x_a + x_b)$, which for small $p_T$ and large $|\bar{y}|$ is approximately $1/2x_a$. Since the parton distributions are relatively well known for large $x$, $R$ can be approximated then by

$$R \sim FG(2p_T/\sqrt{s}\exp(-\bar{y}), p_T^2), \tag{1.4}$$

where $G(x, Q^2)$ denotes the gluon distribution function, and F represents a known function of $p_T$ and $\bar{y}$. From (1.4), it is clear that the value of $R$ at large $\bar{y}$ grows more rapidly for a singular gluon distribution than for a nonsingular distribution.

# 2 Data Analysis

For this analysis, we use approximately $19pb^{-1}$ of data collected by the CDF Collaboration during the 1992-93 run of the Fermilab Tevatron $p\bar{p}$ Collider. The CDF detector and trigger system have been described in detail elsewhere.[1, 2, 3] Here, we note only those changes relevant to this analysis. For the 1992-93 run, in order to span a large range of cross sections, four separate thresholds of 20, 50, 70 and 100 GeV were imposed on the $E_T$ of the trigger clusters. The three lowest thresholds were prescaled to accept 1 in 500, 1 in 20, and 1 in 6 events, respectively. Backgrounds due to cosmic rays have been rejected from the samples.

Jets are identified using the CDF jet-cone algorithm[3], with jet $E_T$'s being measured by summing the energies inside a cone of radius $\sqrt{(\Delta\eta)^2 + (\Delta\phi)^2} = 0.7$. The jet energies have been corrected to account for relative differences in the energy scales between the central calorimeter and the plug and forward calorimeters. Thus, all jets energies are scaled so that the jets appear to have been measured in the central calorimeter. The size of these scale corrections have been determined from dijet balancing studies. Absolute energy scale corrections are not applied, because these effects will be taken into account when the theoretical predictions for $R$ are smeared to incorporate detector effects. After the energy corrections have been applied, the jets are reordered to take account of any shuffling due to the mismeasurement of jet energies close to uninstrumented regions of the detector.

In order to be included in this analysis, the events are required to pass an additional set of cuts that reject residual backgrounds and improve the quality of the data in the samples:

1. The total $E_T$ in the event is required to be less than 2000 GeV, and the missing-$E_T$ fraction, which is defined as $\sqrt{\text{missing-}E_T}/\Sigma E_T$, is required to be less than 6. These cuts are designed to reject the residual cosmic rays and accelerator losses in the data samples.

2. There is a requirement that there be $\geq 1$ primary vertex in the event, and that the event vertex be within 60 cm of the nominal interaction point. This efficiency of this cut has been measured in minimum bias data to be 94.95%.

3. Events containing only one energetic reconstructed jet are discarded by requiring that there be a second jet in the event with corrected $E_T \geq 5$GeV .

| Sample | 15-27 GeV | 27–60 GeV | 60–80 GeV | 80–120 GeV | 120–350 GeV |
|---|---|---|---|---|---|
| SS | 182 | 10335 | 4126 | 6085 | 5296 |
| OS | 171 | 9612 | 4171 | 6357 | 5973 |

Table 1: The number of events in the SS and OS samples having a leading jet in the $E_T$ range specified in the table.

4. The pseudorapidity of the leading jet in the 100 GeV data sample is restricted to the range $|\eta_1| \leq 2.5$. This cut removes residual contamination in the sample from noise in the forward and backward calorimeters, but does not affect the region of physics interest for jet energies $\geq 100$ GeV.

5. A loose back-to-back cut is applied by requiring that $\Delta\phi_{12}$, the azimuthal separation between the first and second jets, lie in the range $\pi - 0.7 \leq \Delta\phi_{12} \leq \pi + 0.7$. This cut removes events with energetic third jets, partially removes events where the second jet energy has been mismeasured and a soft third jet has fluctuated up in energy to take its place, and ensures that the acceptance for SS jet configurations is not cut off by the finite clustering cone size.

In order to make the experimental measurement of $R$, we use the variables $\eta_1$, $\eta_2$, and $E_T$ in place of $y_1$, $y_2$ and $p_T$. For each event, we determine the $E_T$ of the leading jet, and its pseudo-rapidity, $\eta_1$. Events are classified as SS configurations if $\eta_1$ and $\eta_2$ fall into the same $\eta$-bin; they are classified as OS configurations if $|\eta_1|$ and $|\eta_2|$ fall into the same $\eta$-bin, but the sign of $\eta_1$ and $\eta_2$ are opposite. Events are assigned to $E_T$ bins based on the $E_T$ of the leading jet. In order to improve the statistics, we choose the width of the $\eta$ and $E_T$ bins to fairly wide. The $\eta$ bin width is 0.4, which is large compared with the intrinsic $\eta$ resolution of the CDF detector. In order to remove low energy calorimeter noise, the lowest $E_T$-value for the minimum bias data sample is chosen to be 15 GeV. The lowest $E_T$-values for the 20, 50 ,70 and 100 GeV data samples are chosen to correspond to the point at which the trigger becomes approximately 30% efficient for the 20 GeV data sample, and approximately 50% efficient for the others. This choice improves the statistical power of the measurement without increasing the systematic error because the trigger efficiencies cancel in the ratio of the cross sections. Table 1 gives the final number of events in each $E_T$ bin for the SS and OS samples.

For each bin in $E_T$, we determine the measured values of $R$ from the $\eta_1$ distributions

for the SS and OS samples:

$$R(\eta_1, E_T) = \frac{N_{SS}(\eta_1, E_T)}{N_{OS}(\eta_1, E_T)}, \tag{2.5}$$

where $N_{SS}(\eta_1, E_T)$ and $N_{OS}(\eta_1, E_T)$ denote the number of SS and OS jet configurations with the specified kinematics, respectively.

# 3 Results

In Figs. 1–5, we show the measured values of $R$ as a function of $\eta_1$ for the $E_T$ ranges given in Table 1. The measured values are compared with the predictions of LO QCD for the CTEQ2M and CTEQ2MS parton distribution, where the theoretical predictions have been smeared to take into account detector effects. Overall, the data and the smeared predictions are in qualitative agreement. There are some hints that the data favor a singular gluon distribution at small $x$. Although the measured values of $R$ for the higher $E_T$ ranges are not interesting from a small-$x$ point of view, they nevertheless provide a new test of QCD in a previously unmeasured quantity.

From Fig 6, we see that the theoretical prediction for $R$ is very sensitive to the choice of $p_T$. Hence, in order to determine the level of agreement between the data and the theory, it is crucial to understand how the energy scale measured in the data has been affected by the detector response. One can anticipate that energy resolution smearing becomes more important at large $|\eta|$. This is because the slope of the jet-$E_T$ spectrum for a fixed value of $|\eta|$ increases with $|\eta|$, and hence it becomes more likely that one measures a lower $E_T$ jet that has fluctuated up in energy. The detector effects of energy loss and energy resolution smearing have been studied extensively[3, 4], and quantified in the form of detector response functions $R_{CDF}(E_T^{true}, E_T^{meas})$, which give the probability that a jet having some value of true $E_T$, $E_T^{true}$, will fluctuate to a jet with a measured $E_T$, $E_T^{meas}$, in the data. The values of $R_{CDF}$ are known only for the central region of the detector, but we have taken this into account by correcting the jets for relative shifts in the energy scale between the different calorimeter subsystems. The effects of differing resolutions in the plug and forward calorimeters have not yet been included. However, from dijet balancing studies, it is known that these resolutions are comparable to that of the central calorimeter.[5]

In the comparisons between the data and the theoretical predictions shown in Figs.

| | 15-27 GeV | 27–60 GeV | 60–80 GeV | 80–120 GeV | 120–350 GeV |
|---|---|---|---|---|---|
| $p_T$ Range | 5–35 | 15–75 | 40–90 | 60–140 | 80–360 |
| Lum ($nb^{-1}$) | 4.0 | 20.0 | 350. | 2000. | 10000. |

Table 2: The $p_T$ ranges and the luminosities of the simulated data samples.

1–5, we have estimated the effects of the detector response by convoluting the LO QCD predictions for the CTEQ2M and CTEQ2MS parton distributions with the CDF detector response functions. The procedure we use is to begin with a set of theoretical predictions for the SS and OS cross sections in the range $5 \leq p_T \leq 360$. The jet energies are then smeared by the CDF detector response functions using a fast Monte Carlo program to generate a simulated data sample of a given luminosity. Table 2 lists, for each measured $E_T$ bin, the $p_T$ ranges and the luminosities used to generate the simulated data samples. The simulated events are then passed through the data analysis modules in order to determine the predictions for the measured values of $R$.

# 4 Conclusions

We have presented a measurement of the SS-OS dijet cross section ratio for a wide range of measured $E_T$ values, using the full data set from Run Ia. The data have been corrected for relative shifts in the energy scale between the different calorimeter subsystems. We have made a preliminary estimate of the detector effects of energy loss and resolution smearing by folding the theoretical predictions with the known detector response functions. The data are in qualitative agreement with the LO QCD predictions for the values of $R$ in all of the $E_T$ and $\eta$ ranges that have been studied. At present, the measurement is still limited by low statistics, although there is some evidence to support the singular gluon hypothesis.

# References

[1] CDF Collaboration, F. Abe *et al.*, Nucl. Istrum. Methods Phys. Res., Sect. A 271,387 (1988).

[2] CDF Collaboration, F. Abe *et al.*, Phys. Rev. Lett. 62, 613 (1989).

[3] CDF Collaboration, F. Abe *et al.*, Phys. Rev. Lett. 68, 1104 (1992).

[4] CDF Collaboration, F. Abe *et al.*, Phys. Rev. Lett. 70, 1376 (1993).

[5] CDF-note 2608.

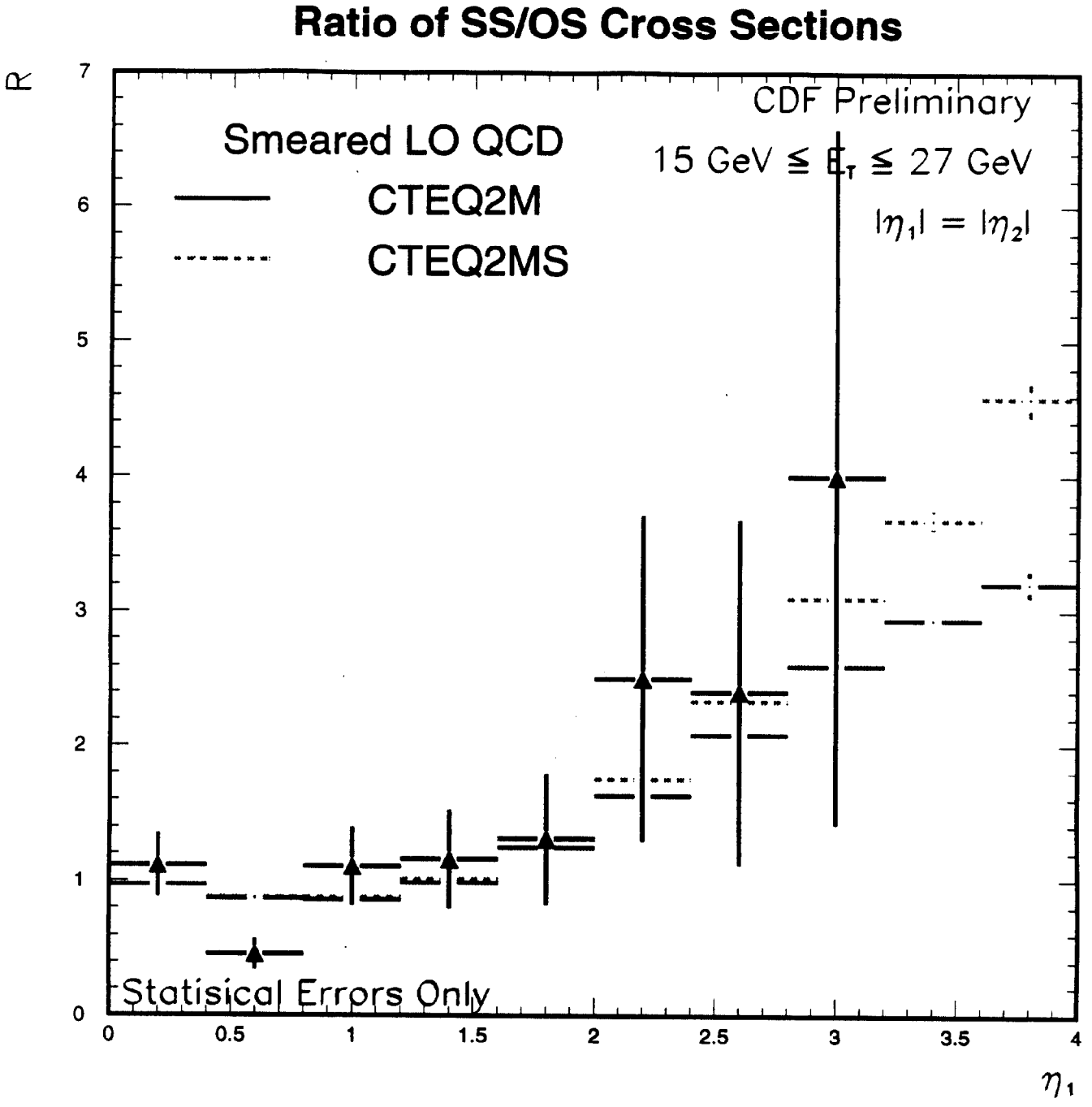


Figure 1: The measured and simulated values of $R$ as a function of $\eta_1$ in the measured $E_T$ range $15 \leq E_T \leq 27$ GeV.

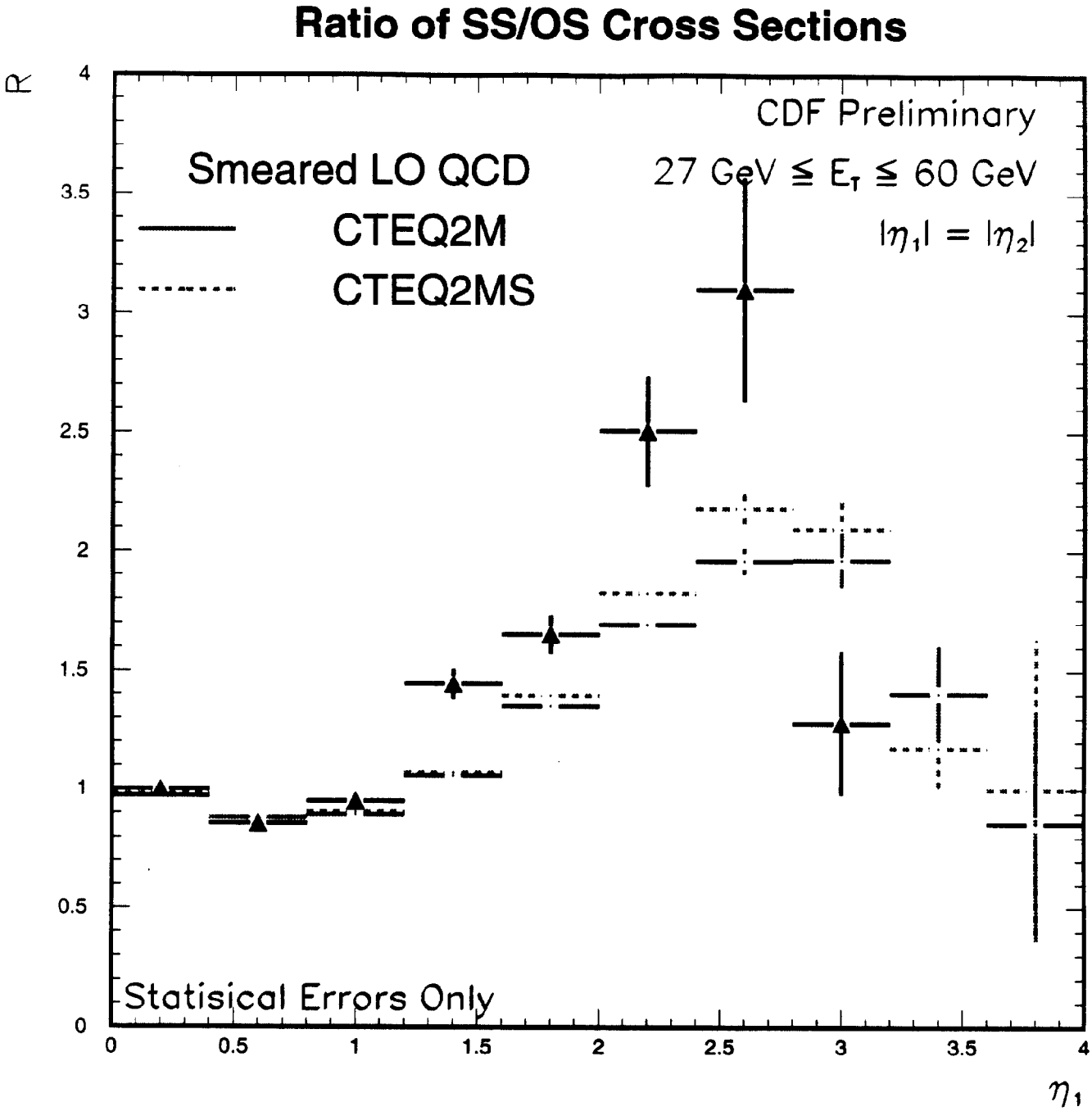


Figure 2: The measured and simulated values of $R$ as a function of $\eta_1$ in the measured $E_T$ range $27 \leq E_T \leq 60$ GeV.

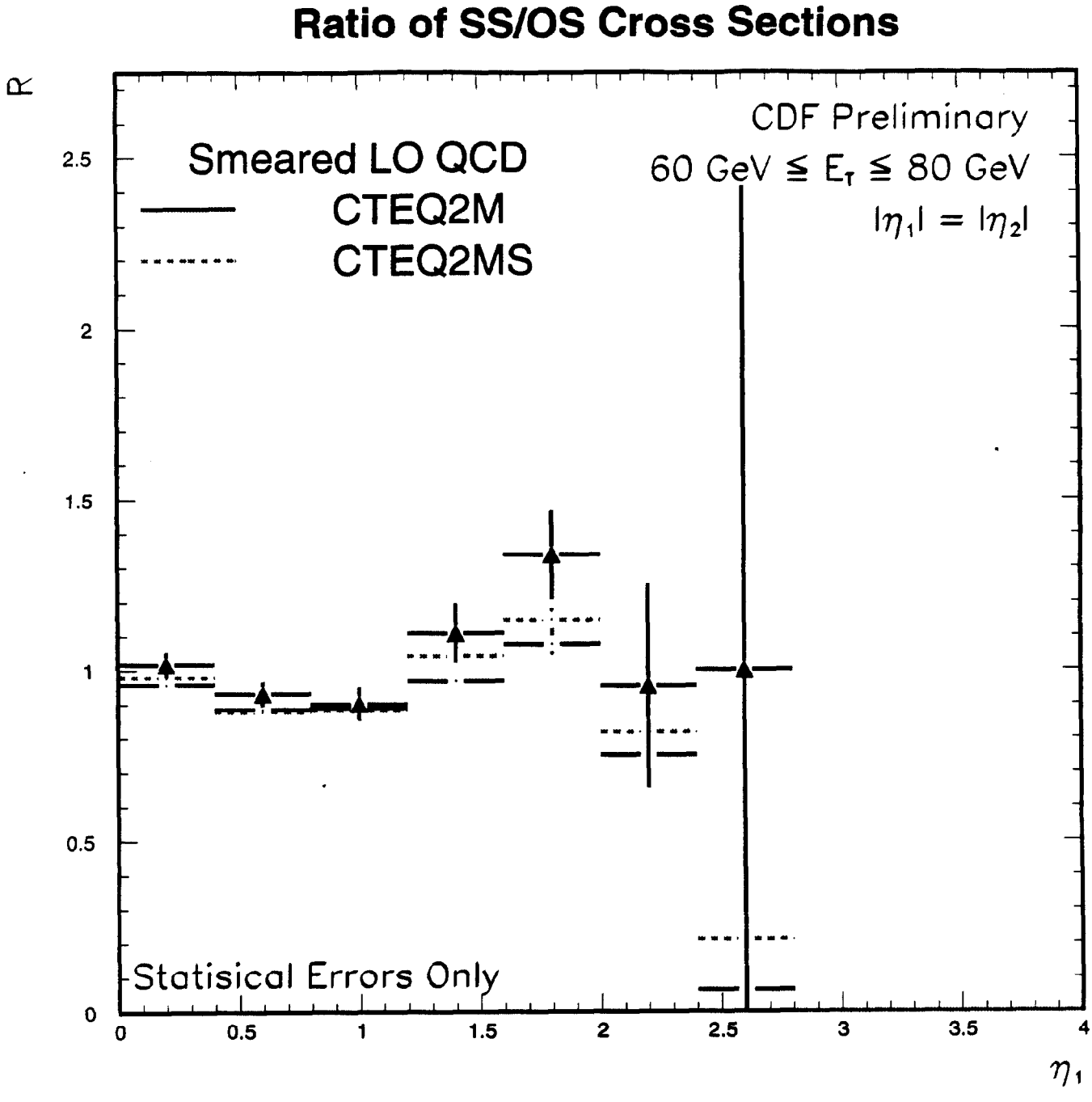


Figure 3: The measured and simulated values of $R$ as a function of $\eta_1$ in the measured $E_T$ range $60 \leq E_T \leq 80$ GeV.

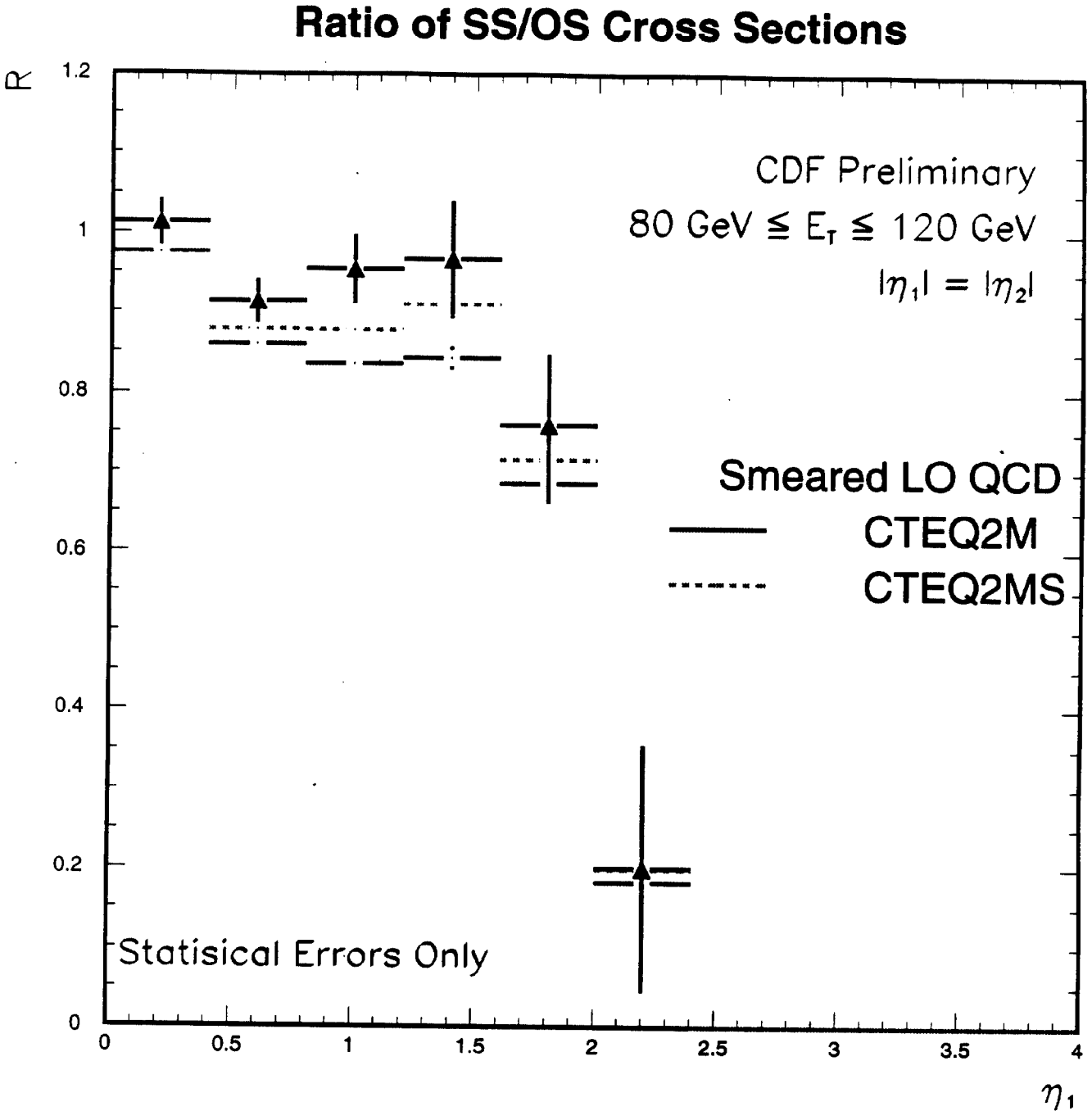


Figure 4: The measured and simulated values of $R$ as a function of $\eta_1$ in the measured $E_T$ range $80 \leq E_T \leq 120$ GeV.

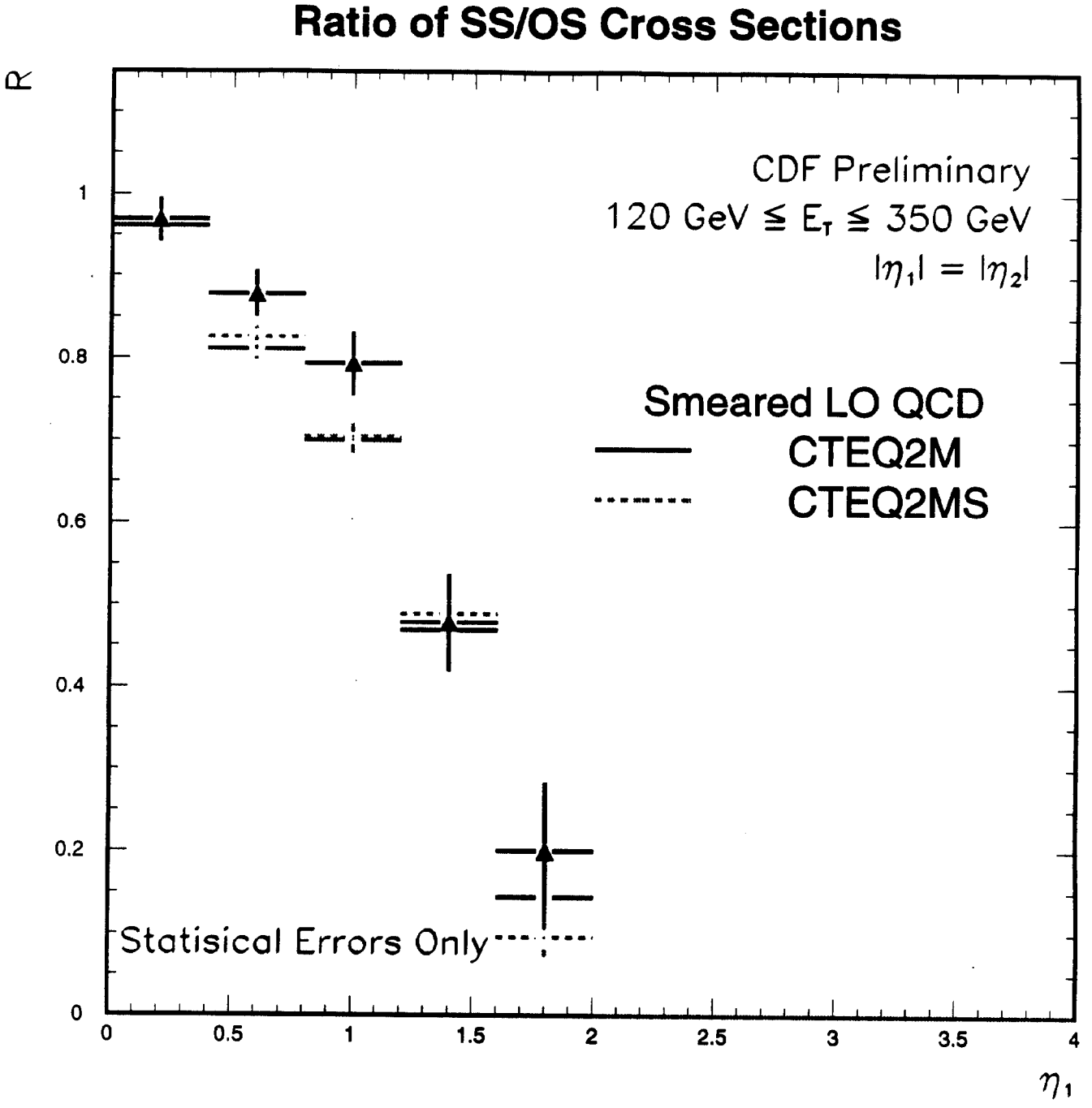


Figure 5: The measured and simulated values of $R$ as a function of $\eta_1$ in the measured $E_T$ range $120 \leq E_T \leq 350$ GeV.

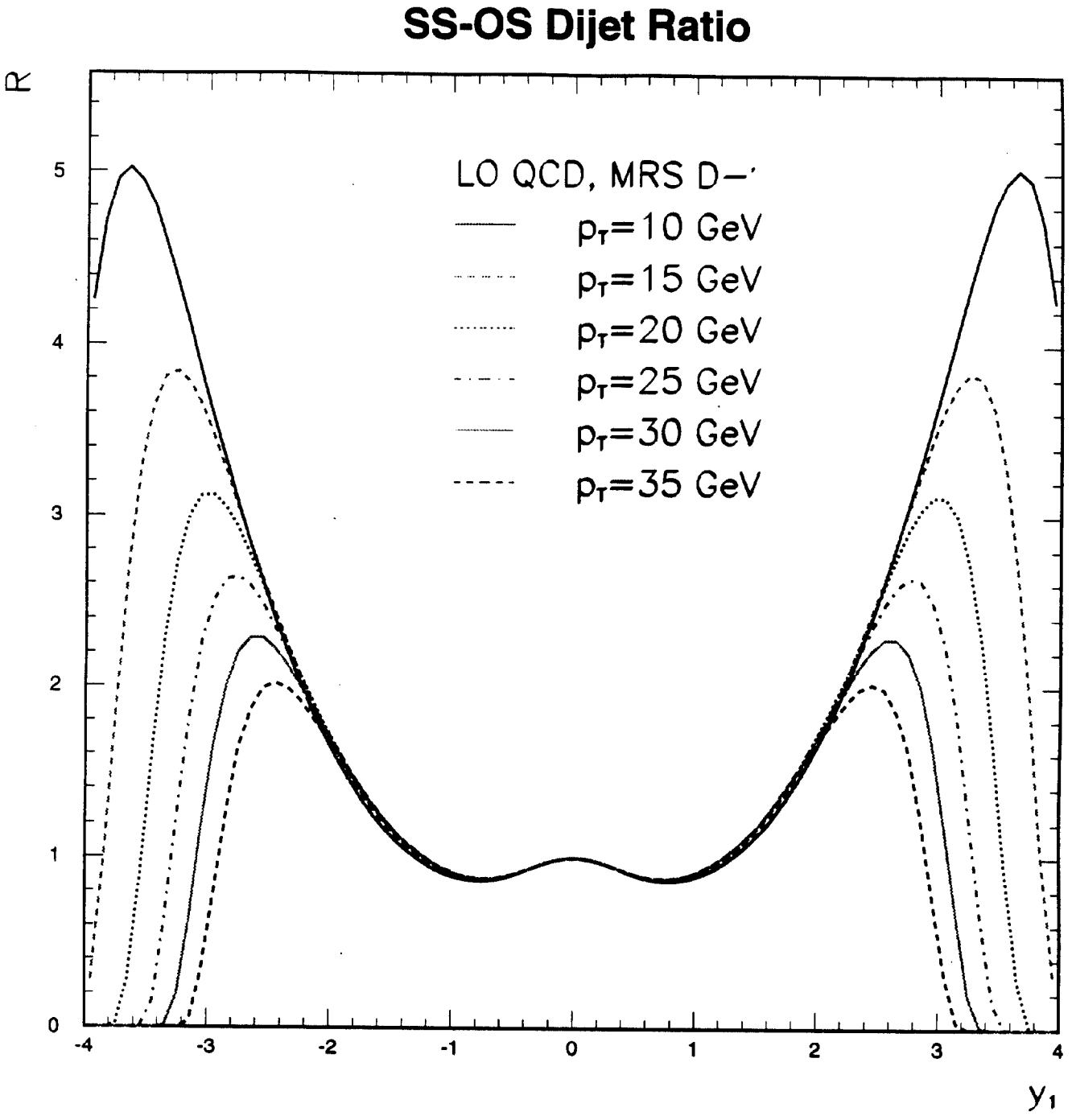


Figure 6: The variation in the LO QCD prediction for the SS-OS dijet ratio for $p_T$ values in the range $15 \leq p_T \leq 35$ GeV. The predictions have been calculated using the MRS D-' parton distribution.